Domain-wall flexing instability and propagation in thin ferromagnetic films

C. Gourdon, L. Thevenard, and S. Haghgoo
Institut des Nanosciences de Paris, Université Pierre et Marie Curie, CNRS, UMR 7588, 4 Place Jussieu, 75005 Paris, France

A. Cēbers
University of Latvia, Zeļļu-8, Rīga, LV-1002, Latvia

(Received 27 March 2013; revised manuscript received 31 May 2013; published 29 July 2013)

We investigate field-driven domain-wall dynamics in thin ferromagnetic layers in the precessional regime using an analytical model that goes beyond the rigid wall approximation and takes into account the flexing modes of domain walls. This model allows us to turn on and off the stray field from domains adjacent to the domain wall in order to elucidate its role. We determine the eigenfrequencies of the flexing modes. The domain-wall flexing instabilities are shown to exist even without the stray field. The amplitude of the flexing modes shows a maximum when the magnetization precession frequency is equal to their eigenfrequency. At maximum amplitude of the flexing modes, the domain-wall velocity exhibits bumps even without the stray field. The stray field further enhances the velocity and broadens the bumps. This study is completed by micromagnetic simulations that show excellent agreement with the analytical model. The role of the various spatial modes in the velocity enhancement is clarified. Additional fractional frequencies appear in the time-dependent amplitude of the flexing modes, in analogy with the behavior of parametric oscillators.

DOI: 10.1103/PhysRevB.88.014428 PACS number(s): 75.60.Ch, 75.78.Cd, 75.70.Ak, 05.45.−a

I. INTRODUCTION

Propagation of magnetic domain walls (DW) attracts a lot of interest in view of potential applications in novel magnetic devices.[1,2] In magnetic films or stripes, following the well-known one-dimensional (1D) model developed in the 70's,[3–5] the DW velocity is expected to rise with the applied magnetic field (stationary regime). After the Walker breakdown, at the Walker field H_W, the velocity shows a nonmonotonous behavior originating from the precession of the magnetization inside the wall (precessional regime). The observation of these intrinsic flow regimes is most often hindered by DW pinning resulting in creep and depinning regimes.[6–9] In some cases (high field, low density of pinning defects), there is clear experimental evidence that the flow regimes can be reached,[7,10–12] thereby allowing for comparison with theory. However experimental results often show deviations from the predicted behavior. An increase of the velocity at certain fields is observed.[10,12–16] A change of the domain-wall structure[14] and the appearance of excitations of internal degrees of freedom on the typical timescale of magnetization precession (e.g., DW width oscillations[17,18] or DW flexing[15]) have been proposed to explain strong velocity enhancements, on the basis of numerical simulations. For in-plane magnetized materials,[17,18] no mechanism has been put forward to relate these two observations. In perpendicularly magnetized materials, a toy model has been suggested using a simple analytical description of the flexing DW structure.[15] For large Gilbert damping, it identified some of the velocity bumps as the resonance of the first flexural mode and its coupling to the stray field from the domains adjacent to the wall. Exploring smaller values of this damping constant might lead to novel features in the DW dynamics because of the intrinsic nonlinearity in the Landau-Lifshitz-Gilbert equation at the basis of DW propagation equations. In particular one expects the appearance of higher order flexing modes but also of additional frequencies in the spectrum of magnetization precession, typical of a parametric oscillator behavior.[19]

Efficient excitation of new internal degrees of freedom becomes possible at the onset of DW instabilities. Theoretically, DW instabilities in ferromagnetic films were investigated in special cases: orthorhombic anisotropy,[20,21] with an applied field in the film plane,[22] or close to the anisotropy field.[23,24] However their contribution to DW dynamics was not studied in detail. A clear understanding of the role of instabilities in more standard geometries and in the entire field range currently investigated in DW propagation experiments (precessional regime) is still lacking. Actually, several types of instabilities may be considered: flexing modes in the thickness of the film, corrugation, or buckling along the DW plane.[22,25]

In this paper we concentrate on the first type of instabilities: flexing modes and the associated magnetization twist in the film thickness. We consider perpendicularly magnetized layers. Within the general framework of collective coordinates,[3,17,18] we develop an analytical model that takes into account the spatial and temporal dependencies of the DW profile and precession angle, thereby extending the approach beyond the 1D model that described a rigid wall with uniform precession. Within this model the stray field of the domains can be turned on and off in order to get a deeper insight into its precise role. We thereby show that the flexing instabilities of the precession motion of the magnetization in the DW exist regardless of the action of the stray field even though the mode amplitudes depend on the stray field. Furthermore this model shows that a reduced set of parameters is sufficient to describe the DW dynamics with DW flexing.

From micromagnetic simulations we then obtain velocity curves which are very similar to the analytical model, showing the relevance of this model despite an approximate expression of the stray field. We clarify the respective contribution of the various oscillation modes to the velocity peaks. With

decreasing damping constant an additional high velocity plateau appears in the precessional regime, in agreement with experimental findings. At velocity peaks novel frequencies, namely subharmonics of the fundamental precessional frequency, appear in the frequency spectrum of the oscillation modes. This is reminiscent of frequency locking at a rational multiple of the eigenfrequency for parametric oscillators.[19,26,27]

The paper is organized as follows. Section II presents the analytical model. We first obtain a set of partial differential equations (PDE) for the coupled variables, DW profile, and precessional angle. The analysis of the DW flexing instabilities in the framework of linear theory reduces to the calculation of the Floquet multipliers.[26] Section III describes the results of micromagnetic simulations. In Sec. IV we summarize the results and give a few perspectives.

II. ANALYTICAL MODEL

A. Equations of motion for a flexing DW

We consider a ferromagnetic layer in the x-y plane, with thickness d along the z direction and infinite length along the x and y directions (Fig. 1). The magnetic field is applied along z (the magnetic easy axis) and the DW propagates along y. We assume that the DW z profile is invariant along x. The analysis of the stability of the DW motion is carried out on the basis of the equations derived in Ref. 3. The DW magnetization is represented as $\vec{M} = M(\sin\theta\cos\varphi,\ \sin\theta\sin\varphi,\ \cos\theta)$ using the reference frame of Fig. 1. The Landau-Lifshitz-Gilbert equation for the magnetization

$$\dot{\vec{M}} = \gamma \vec{M} \times \frac{\delta E}{\delta \vec{M}} + \frac{\alpha \vec{M} \times \dot{\vec{M}}}{M}, \tag{1}$$

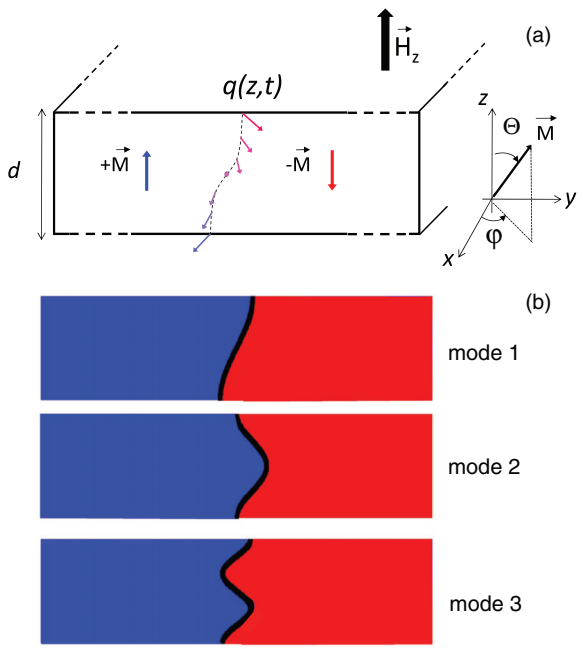

FIG. 1. (Color online) (a) Schematic of the sample film (side view) and definition of the notations used in the text. (b) Profiles of the three first flexural modes of the DW.

with γ the gyromagnetic factor ($\gamma > 0$), is analyzed by splitting the energy density E of the ferromagnet into two parts $E = E_0 + E_1$. The first one includes the exchange energy (exchange constant A) and anisotropy energy (anisotropy constant K)

$$E_0 = A\left[\left(\frac{\partial\theta}{\partial y}\right)^2 + \sin^2\theta\left(\frac{\partial\varphi}{\partial y}\right)^2\right] + K\sin^2\theta. \tag{2}$$

The second part E_1 accounts for the interaction with the external field along the z axis that causes DW propagation, the stray field from adjacent domains, the DW local demagnetizing field, and the increase of the DW energy due to its flexing

$$\begin{aligned} E_1 = &-MH_z\cos\theta - M\sin\theta\sin\varphi H_y^{sf}(z) \\ &+ 2\pi M^2\sin^2\theta\sin^2\varphi \\ &+ A\left[\left(\frac{\partial\theta}{\partial z}\right)^2 + \sin^2\theta\left(\frac{\partial\varphi}{\partial z}\right)^2\right], \end{aligned} \tag{3}$$

where[28] $H_y^{sf}(z) = Mh^{sf}(z)$ and

$$\begin{aligned} h^{sf}(z) = 2\ln\left[\frac{z^2 + (\Delta/2)^2}{(d-z)^2 + (\Delta/2)^2}\right] + \frac{8}{\Delta}\Bigg[z\arctan\left(\frac{\Delta}{2z}\right) \\ - (d-z)\arctan\left(\frac{\Delta}{2(d-z)}\right)\Bigg], \end{aligned} \tag{4}$$

where $\Delta = \sqrt{A/K}$ is the DW width. Equation (1) in the steady state at $E_1 = 0$ has a standard solution $\theta = \theta_0(y - q)$ and $\varphi = \varphi_0$, where q and φ_0 are collective coordinates.[17,18] We have $d\theta_0/dy = \sin\theta_0/\Delta$. Terms in E_1 are accounted for as perturbation. The solutions are sought in the form $\theta = \theta_0(y - q) + \theta_1$ and $\varphi = \varphi_0 + \varphi_1$.

In the first order we have

$$\begin{aligned} \frac{\gamma}{M}\frac{\delta\left(E_0^0 + E_0^1 + E_1\right)}{\delta\theta} &= -\alpha\dot{\theta}_0 + \dot{\varphi}_0\sin\theta_0 \\ \frac{\gamma}{M}\frac{\delta\left(E_0^0 + E_0^1 + E_1\right)}{\delta\varphi} &= -\alpha\dot{\varphi}_0\sin^2\theta_0 - \dot{\theta}_0\sin\theta_0, \end{aligned} \tag{5}$$

where E_0^1 is the correction to the energy E_0 due to the first order terms. Equation (5) gives

$$\begin{aligned} &\frac{\gamma}{M}\left(-2A\frac{d^2\theta_1}{dy^2} + 2K\theta_1\cos 2\theta_0\right) \\ &\quad = \frac{\gamma}{M}\frac{\delta E_0^1}{\delta\theta} = -\alpha\dot{\theta}_0 + \dot{\varphi}_0\sin\theta_0 - \frac{\gamma}{M}\frac{\delta E_1}{\delta\theta}; \\ &\frac{\gamma}{M}\left[-2A\frac{d}{dy}\left(\frac{d\varphi_1}{dy}\sin^2\theta_0\right)\right] \\ &\quad = \frac{\gamma}{M}\frac{\delta E_0^1}{\delta\varphi} = -\alpha\dot{\varphi}_0\sin^2\theta_0 - \dot{\theta}_0\sin\theta_0 - \frac{\gamma}{M}\frac{\delta E_1}{\delta\varphi}. \end{aligned} \tag{6}$$

Since $\delta E_0^1/\delta\theta = 0$ and $\delta E_0^1/\delta\varphi = 0$ have the solutions φ_1 independent on y and $\theta_1 \propto d\theta_0/dy$, then similarly to the method developed in Ref. 29, the solvability condition of the set of linear equations (6) for θ_1 and φ_1 with the natural boundary conditions $\theta_{1,z}|_{z=0,d} = \varphi_{1,z}|_{0,d} = 0$ reads

$$\int_{-\infty}^{\infty}\frac{d\theta_0}{dy}\frac{\delta E_0^1}{\delta\theta}dy = 0; \quad \int_{-\infty}^{\infty}\frac{\delta E_0^1}{\delta\varphi}dy = 0. \tag{7}$$

As a result, the equations for the center line of the domain wall $q(z,t)$ and the precession angle $\varphi(z,t)$ are as follows:

$$\dot{\varphi} = h_w - \sin 2\varphi + \frac{h^{sf}(z)}{4}\cos\varphi + 2\Lambda^2\varphi_{zz} + \frac{2\Lambda^2}{\alpha^2}\tilde{q}_{zz}; \quad (8)$$

$$\dot{\tilde{q}} = \alpha^2 h_w + \sin 2\varphi - \frac{h^{sf}(z)}{4}\cos\varphi + 2\Lambda^2\tilde{q}_{zz} - 2\Lambda^2\varphi_{zz}, \quad (9)$$

where $\tilde{q}$ is equal to $\alpha q/\Delta$, the subscript zz denotes the second spatial derivative, $\Lambda = \sqrt{A/2\pi M^2}$ is the exchange length, h_w stands for H_z/H_W where $H_W = \alpha 2\pi M$ is the Walker field, and time is in units of $(1+\alpha^2)/\gamma H_W$. We can see that the most important parameters are the ratio of the layer thickness to the exchange length d/Λ and the damping α. The DW width Δ simply renormalizes the DW displacement and the magnetization M gives the field unit, for the applied and stray fields.

In the spatially homogeneous case when the stray field is neglected (rigid wall, 1D model) and $h_w > 1$, Eq. (8) has a periodic solution φ_0 that reads

$$\tan\varphi_0 = \frac{1}{h_w} + \sqrt{1 - \frac{1}{h_w^2}}\tan\left(\sqrt{h_w^2 - 1}t\right). \quad (10)$$

The fundamental frequency in the Fourier spectrum of φ_0 is $f_0 = \sqrt{h_w^2 - 1}/\pi$, the precession frequency is $f_p = f_0/2$. The oscillatory behavior entirely results from the DW local demagnetizing field [the $\sin 2\varphi$ term in Eq. (8)]. The stability of this precession regime with respect to DW flexing is considered in the next section.

B. Flexing instability

The equations for the small flexing perturbations $\delta\varphi$, $\delta\tilde{q}$ read

$$\delta\dot{\varphi} = -2\delta\varphi\cos 2\varphi_0(t) + 2\Lambda^2\delta\varphi_{zz} + \frac{2\Lambda^2}{\alpha^2}\delta\tilde{q}_{zz} \quad (11)$$

$$\delta\dot{\tilde{q}} = 2\delta\varphi\cos 2\varphi_0(t) - 2\Lambda^2\delta\varphi_{zz} + 2\Lambda^2\delta\tilde{q}_{zz}. \quad (12)$$

The most simple approach to analyze the evolution of the small flexing perturbations is to develop them into series $\delta\varphi = \sum_{n=1}^{\infty}\varphi_n(t)\cos(n\pi z/d)$ and $\delta\tilde{q} = \sum_{n=1}^{\infty}\tilde{q}_n(t)\cos(n\pi z/d)$ that satisfy the natural boundary conditions and to study the time evolution of the amplitudes of modes $[\varphi_n(t), \tilde{q}_n(t)]$. The set of equations for the amplitudes φ_n and $\tilde{q}_n$ reads $(k_n = n\pi/d)$:

$$\dot{\varphi}_n + 2\Lambda^2 k_n^2\left(\varphi_n + \frac{\tilde{q}_n}{\alpha^2}\right) = -2\varphi_n\cos 2\varphi_0(t), \quad (13)$$

$$\dot{\tilde{q}}_n - 2\Lambda^2 k_n^2(\varphi_n - \tilde{q}_n) = 2\varphi_n\cos 2\varphi_0(t). \quad (14)$$

When dropping the $\cos(2\varphi_0(t))$ driving term one obtains the complex angular eigenfrequencies of the spatial modes $(\pm 1 + i\alpha)\omega_n$ with $\omega_n = 2\pi^2 n^2(\Lambda/d)^2/\alpha$ in reduced units. The modes eigenfrequencies are then

$$f_n = n^2(\Lambda/d)^2\pi(\gamma 2\pi M)/(1+\alpha^2). \quad (15)$$

Note that, when setting the damping term to zero, this expression represents the thin film limit of the DW free-oscillation frequency obtained by Slonczewski.[5,25]

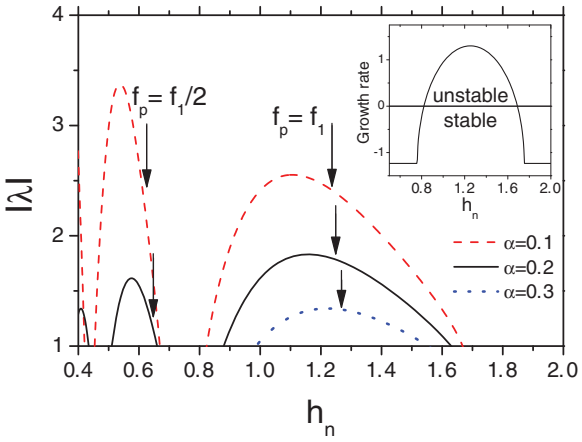

FIG. 2. (Color online) Field dependence of the Floquet multiplier for mode 1 ($h_n = H_z/2\pi M$). Long dashed line $\alpha = 0.1$, solid line $\alpha = 0.2$, and short dashed line $\alpha = 0.3$. The layer thickness is $d/\Lambda = 4$. The arrows indicate the fields at which the precession frequency is equal to f_1 or $f_1/2$, f_1 being the eigenfrequency of the first flexural and precessional modes [Eq. (15)]. The inset shows the growth rate of mode 1 calculated from the parametric oscillator model [Eq. (19)] for $\alpha = 0.2$ and $d/\lambda = 4$.

The existence of increasing-in-time solutions of Eqs. (13) and (14) is analyzed by the calculation of the Floquet multipliers.[26] For the vector of dynamic variables $Y = (\varphi_n, \tilde{q}_n)$ the equation in matrix form is obtained as

$$\dot{Y}(t) = A(t)\cdot Y(t). \quad (16)$$

Its solution at $t = T_0 = \pi/\sqrt{h_w^2 - 1}$ may be written as $Y(T_0) = B\cdot Y_0$, where B is a monodromy matrix

$$B = \prod_{i=1}^{k}\exp\left[A\left(\frac{t_i + t_{i+1}}{2}\right)\Delta t\right],$$

and $Y(0) = Y_0$; $t_0 = 0$, $t_{k+1} = T_0$ and Δt is the time step. The eigenvalues λ of the 2×2 matrix B give the Floquet multipliers. If $|\lambda| > 1$ the perturbations in the form of the corresponding eigenfunction of the matrix B grow. The Floquet multipliers for mode $n = 1$ for several values of the dissipative parameter α at $d/\Lambda = 4$ are shown in Fig. 2 ($k = 400$). The values of α are chosen in a range which is relevant for ferromagnetic semiconductors.[10] We find that there is a range of field $h_n = H_z/2\pi M$ between 1 and 1.6, weakly depending on α, where the flexing instability occurs. The field value at which the precession frequency f_p is equal to the eigenfrequency f_1 of mode 1 is indicated by an arrow in Fig. 2. It falls well inside the instability region. We also see in Fig. 2 that a narrower instability range develops around $f_p = f_1/2$.

The system described by Eqs. (13) and (14) is similar to the parametrically excited oscillator as we explain below. Putting $\varphi_n = \exp(-\alpha\omega_n t)a$, $\tilde{q}_n = \exp(-\alpha\omega_n t)b$ and introducing a small parameter ε we can consider a model system:

$$\dot{a} = -\frac{\omega_n}{\alpha}b - 2\varepsilon\cos[2\varphi_0(t)]a,$$
$$\dot{b} = \alpha\omega_n b + 2\varepsilon\cos[2\varphi_0(t)]a. \quad (17)$$

The time-dependent term in Eqs. (17) is given by its Fourier series ($\omega = \sqrt{h_w^2 - 1}$):

$$\cos[2\varphi_0(t)] = \sum_{n=1}^{\infty}[c_n \cos(2n\omega t) + d_n \sin(2n\omega t)].$$

For the case of small values of the parameter ε Eqs. (17) may be solved by the method of multiple time scales. Looking for the solution for variable a as $a(t) = A(T)\cos(\omega t) + B(T)\sin(\omega t)$ with $T = \varepsilon t$ and introducing a small detuning $\Delta\omega$

$$(\omega_n)^2 \simeq \omega^2 + 2\varepsilon\omega\Delta\omega,$$

the condition of the absence of the secular terms in the equation for the first order in ε gives

$$\begin{aligned}\frac{dA}{dT} &= \Delta\omega B + \frac{1}{2}\left(\frac{1}{\alpha}d_1 - c_1\right)A - \frac{1}{2}\left(\frac{1}{\alpha}c_1 + d_1\right)B,\\ \frac{dB}{dT} &= -\Delta\omega A - \frac{1}{2}\left(\frac{1}{\alpha}c_1 + d_1\right)A - \frac{1}{2}\left(\frac{1}{\alpha}d_1 - c_1\right)B.\end{aligned} \tag{18}$$

As a result for the largest growth rate σ_n of the flexing modes $(\varphi_n, \tilde{q_n})$ we have

$$\sigma_n = -\alpha\omega_n + \varepsilon\sqrt{\frac{1}{4}\left(\frac{1}{\alpha^2} + 1\right)\left(c_1^2 + d_1^2\right) - (\Delta\omega)^2}. \tag{19}$$

The growth rate given by relation (19) for mode 1 ($n = 1$) is shown in the inset of Fig. 2. It is positive (unstable mode with growing amplitude) in the same range of field strength as the instability obtained by the calculation of the Floquet multipliers.

Returning to the Floquet multipliers, the dependence of the instability range on the layer thickness is illustrated in Fig. 3. With the decrease of the film thickness the instability regions shift to larger magnetic field and are less expressed since the Floquet multipliers have smaller values. This is fully consistent with our previous results from micromagnetic simulations.[15]

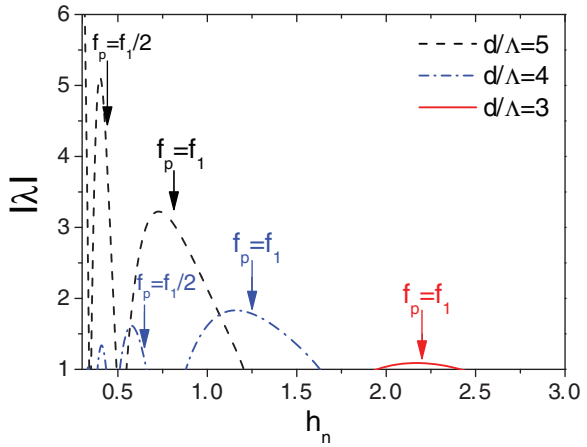

FIG. 3. (Color online) Field dependence of the Floquet multiplier for mode 1 for different thicknesses of the film. Long dashed line $d/\Lambda = 5$, dash-dotted line $d/\Lambda = 4$, and solid line $d/\Lambda = 3$. $\alpha = 0.2$. The arrows indicate the fields at which the precession frequency is equal to f_1 or $f_1/2$, f_1 being the eigenfrequency of the first flexural and precessional modes [Eq. (15)].

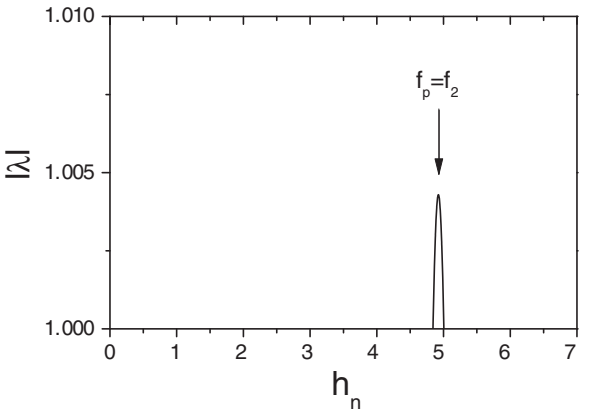

FIG. 4. The Floquet multiplier for the second flexing mode. $\alpha = 0.1$, $d/\Lambda = 4$.

Interestingly, besides the instability with respect to the first mode there is also an instability with respect to the second mode in a narrow range of field strength at small values of the dissipative parameter. This instability occurs when the precession frequency is equal to the second mode eigenfrequency f_2. The corresponding values of the Floquet multipliers are shown in Fig. 4 ($\alpha = 0.1$). The rate of growth is small therefore many periods are necessary for this instability to grow. This instability corresponds very well to the abrupt onset of a large mode amplitude and enhanced velocity at $h_n = 5$ that sets up after several tens of nanoseconds, as found from simulations (see Sec. III).

The flexing instability of the DW in the precession regime causes bumps in the DW velocity curve. This is illustrated in Fig. 5 where the thickness and time-averaged DW velocity is shown as a function of the field strength. The average velocity is calculated by discretization of Eqs. (8) with finite differences

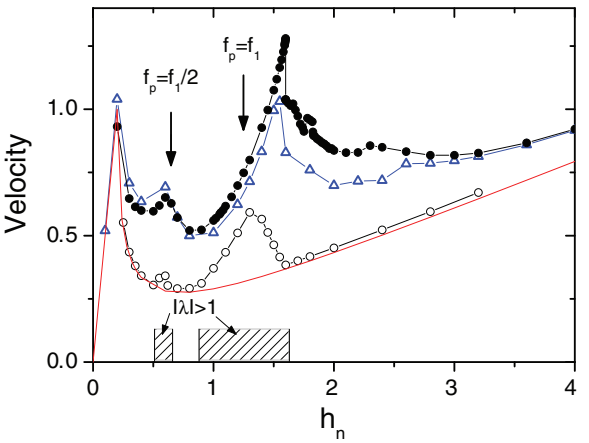

FIG. 5. (Color online) DW velocity v (averaged over film thickness and precession period) as a function of field strength. Calculation according to PDE [Eqs. (8)] with the stray field (solid circles) and without (open circles), calculation by the reduced set of equations [Eqs. (22)–(25)] (triangles), 1D model (full curve). The dashed areas represent the instability regions. The arrows indicate the fields at which the precession frequency is equal to f_1 or $f_1/2$, f_1 being the eigenfrequency of the first flexural and precessional modes [Eq. (15)]. The parameters are $\alpha = 0.2$, $d/\Lambda = 4$, $\Delta/\Lambda = 0.3$.

and solving for the variables $\varphi_{z_i}, q_{z_i}; (i = 1, \ldots, n+1)$ on the uniform grid with $n = 200$ mesh points by an implicit algorithm with the reduced time step 10^{-2}. The positions of the bumps correlate quite well with the range of field strength where flexing instabilities take place. The velocity bumps develop even in the absence of the stray field (open circles in Fig. 5). However the bumps appear in a narrow field range and the velocity curve remains quite close to the 1D model. The action of the stray field further enhances the velocity over a broader field range (solid circles in Fig. 5).

The largest velocity bump develops when the precession frequency is equal to the eigenfrequency of the first mode. A similar correlation is observed for other values of the dissipative parameter α (not shown). The excitation of the first flexing mode allows us to propose a reduced description of the DW propagation based on the series for φ and q where only the first flexing mode is taken into account

$$\varphi(t,z) = \varphi_0(t) + \varphi_1(t)\cos(\pi z/d), \tag{20}$$

$$\alpha q(t,z)/\Delta = \tilde{q}_0(t) + \tilde{q}_1(t)\cos(\pi z/d). \tag{21}$$

The reduced set of equations reads

$$\dot{\varphi_0} = h_w - \sin(2\varphi_0)J_0(2\varphi_1) - \sin(\varphi_0)f(\varphi_1); \tag{22}$$

$$\dot{\varphi_1} = -2\cos(2\varphi_0)J_1(2\varphi_1) - \frac{\omega_1}{\alpha}\tilde{q}_1 - \alpha\omega_1\varphi_1 + 2\cos(\varphi_0)g(\varphi_1); \tag{23}$$

$$\dot{\tilde{q}_0} = \alpha^2 h_w + \sin(2\varphi_0)J_0(2\varphi_1) + \sin(\varphi_0)f(\varphi_1); \tag{24}$$

$$\dot{\tilde{q}_1} = 2\cos(2\varphi_0)J_1(2\varphi_1) - \alpha\omega_1\tilde{q}_1 + \alpha\omega_1\varphi_1 - 2\cos(\varphi_0)g(\varphi_1), \tag{25}$$

where

$$f(\varphi_1) = \frac{1}{d}\int_0^d \frac{h^{sf}(z)}{4}\sin[\varphi_1\cos(\pi z/d)]dz;$$
$$g(\varphi_1) = \frac{1}{d}\int_0^d \cos(\pi z/d)\frac{h^{sf}(z)}{4}\cos[\varphi_1\cos(\pi z/d)]dz. \tag{26}$$

The DW velocity v averaged over the film thickness and the precession period is calculated according to Eqs. (22)–(25) and displayed in Fig. 5 (triangles) as a function of the field strength. The results agree quite well with those obtained from the solution of the PDE [Eq. (8)] (solid circles). This justifies the analysis of the DW propagation obtained in Ref. 15 considering only the first flexing mode. The velocity enhancement arises to a large extent from the $\sin\varphi_0 f(\varphi_1)$ term in Eq. (24). Since the stray field function $h^{sf}(z)$ is odd with respect to the mid-plane of the layer, the function f defined by Eq. (26) takes nonzero values only for odd spatial modes (modes 1 and 3 but mode 3 has a negligible amplitude). This is the reason why, although mode 2 might have a large amplitude or may trigger a new regime by its instability (as found from the analysis of the Floquet multiplier around $h_n = 5$), the velocity is enhanced only if mode 1 has a large amplitude. Actually from Fig. 5 one can see the contribution of higher order modes as the difference between the two curves (solid circles and triangles) in the range $h_n = 1$–3.

One important result of this section is that the instabilities of the flexing modes are found to exist even without the stray field from the domains. These instabilities are driven by the DW demagnetization field [the $\sin(2\varphi)$ term in Eq. (8) or correspondingly the $\cos(2\varphi_0(t))$ term in Eqs. (11) and (12)]. A large amplitude of flexing modes gives rise to bumps in the velocity curve when the precession frequency matches their eigenfrequency. The action of the stray field on magnetization precession inside the wall further enhances the velocity.

It is interesting to note the similarities between our results and the propagation of a vortex wall in a ferromagnetic track with in-plane magnetization.[17,18] The periodic movement of the vortex core in the transverse direction, bouncing between the track edges is analogous to the φ precession. Velocity enhancement is also found when additional modes are excited, in that case oscillations of the vortex wall width.

C. Fractional frequencies

The parametric instability of the DW propagation considered above allows one to understand the rather complicated DW dynamics observed in experiments and found hereafter from numerical simulations (Sec. III). One such peculiarity is the appearance of the fractional frequencies nf_p/p (with n and p integers) in the spectrum of dynamic variables. There are ranges of field strength where these fractional frequencies are observed. For instance frequencies $2f_p/3$ and $4f_p/3$ appear in the Fourier spectrum of the second flexing mode for $\alpha = 0.1$ and $d/\Lambda = 4$, in the same field range where these frequencies are observed in micromagnetic simulations, $h_n = 1.5$–2. The development of fractional frequencies is characteristic of synchronization phenomena where nonlinear oscillators synchronize the period of their oscillations to an external forcing.[19,30] For the above example the fractional frequencies appear in the field range where the precession frequency is equal to $3f_1/2$, i.e., three periods of precession equal to two periods of the first eigenmode. A similar situation was recently encountered in magnetic vortex dynamics when the vortex gyration frequency is commensurate with the vortex core reversal frequency.[31]

III. DOMAIN-WALL DYNAMICS FROM MICROMAGNETIC SIMULATIONS

A. Parameters

In order to assess the validity of the above model given the approximate description of the stray field we performed micromagnetic simulations to obtain a full record of the domain-wall profile, magnetization, and velocity. The simulations are performed using the open source OOMMF package.[32] The geometry of the layer is the one depicted in Fig. 1. A mesh with 2×2 nm^2 cells is used. Magnetic images containing the magnetization unit vector (m_x, m_y, m_z) in each cell are generated at every time step and field step. For each image, from the m_i values averaged over the DW width we obtain the depth-dependent position of the DW $q(z)$ and the azimuthal angle $\varphi(z)$. For most of the following results the sample parameters are chosen in order to investigate

the case where at least two flexural modes are excited. The sample thickness d, the exchange length Λ, and the DW thickness Δ are chosen such that $d/\Lambda = 4$ and $\Delta/\Lambda = 0.3$. This choice leads to the following parameters: magnetization $M = 39.9$ kA m^{-1}, exchange constant $A = 10^{-13}$ J m^{-1}, anisotropy constant (along z) $K = 1.1 \times 10^4$ J m^{-3}, and thickness $d = 40$ nm. These parameters are typical for, e.g., a ferromagnetic semiconductor like GaMnAs.[33] The sample length L along the y direction is 2 μm (4 μm when a long propagation time is needed). Two values have been used for the damping parameter: $\alpha = 0.2$ and 0.1, in agreement with typical values obtained from DW propagation experiments.[10,15] For the sake of comparison with the analytical model the magnetic field strength will be normalized as $h_n = \alpha H/H_W = 2H/M$ ($H/2\pi M$ in cgs units).

The simulation starts with the z-averaged value of m_z, $\langle m_z\rangle_z$, equal to 0, the DW being centered at $L/2$. $\langle m_z\rangle_z$ is equal to 1 when the DW reaches the end of the sample. Therefore, the DW velocity v is obtained as $(L/2)\frac{d}{dt}\langle m_z\rangle_z$ in the stationary regime or as the time average of this quantity over several tens of periods in the precessional regime.

B. Velocity curve and flexural modes

Figure 6(a) displays the DW velocity resulting from simulation as a function of the applied field. The red line represents the 1D model. After the Walker peak at 5 mT ($h_n = 0.2$) the velocity decreases but not as much as expected within the 1D model then it rises again, showing two bumps at $h_n = 1.2$ and 2 and finally meets the 1D curve above $h_n = 4$. It was shown in a previous work that for a large damping (0.3) only one velocity bump remains and shifts to higher fields as the film thickness is decreased.[15]

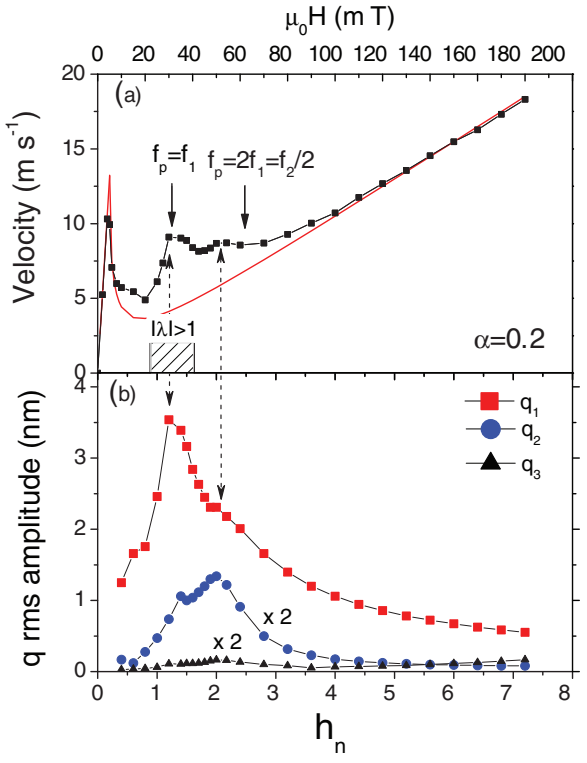

FIG. 6. (Color online) (a) DW velocity as a function of the applied magnetic field, 1D-model (red line), micromagnetic simulation (squares) using $d/\Lambda = 4$, $\Delta/\Lambda = 0.3$, and $\alpha = 0.2$. (b) Amplitudes (rms values) of the first three flexural modes q_1, q_2, and q_3 of the DW.

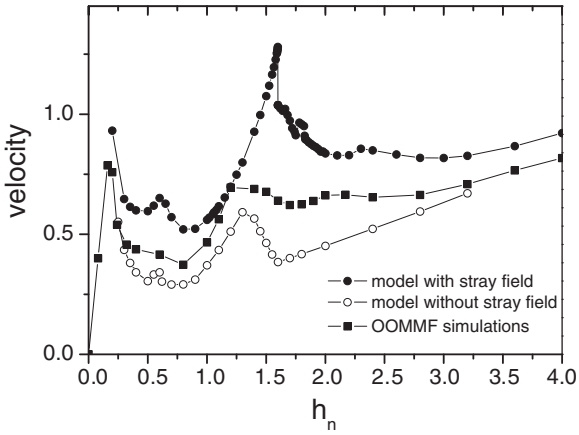

FIG. 7. (a) DW velocity as a function of the applied magnetic field, micromagnetic simulations (squares), calculation according to PDE [Eqs. (8)] with the stray field (solid circles), and without (open circles). The parameters are $d/\Lambda = 4$, $\Delta/\Lambda = 0.3$, and $\alpha = 0.2$.

Figure 7 shows the velocity curve obtained from the micromagnetic simulations together with the velocity curves obtained from the model [Eqs. (8)] with and without the stray field from the domains (solid and open circles, respectively). Without the stray field the velocity is underestimated. With the stray field it is overestimated, which likely comes from the approximate expression of the stray field in the analytical model [Eq. (4)] and from the expression of the DW local demagnetization film that neglects volume magnetic charges appearing from DW flexing.[5]

The DW profile $q(z,t)$ and precession angle $\varphi(z,t)$ obtained from micromagnetic simulations are excellently fitted with a sum of four spatial modes: $q(z,t) = \sum_{n=0}^{4} q_n(t)\cos(n\pi z/d)$ and $\varphi(z,t) = \sum_{n=0}^{4} \varphi_n(t)\cos(n\pi z/d)$. Since the $q_n(t)$ and $\varphi_n(t)$ generally contain several frequency components it is convenient to characterize their amplitude by the root-mean-square (rms) value. Figure 6(b) displays the amplitude of the flexural modes q_1, q_2, and q_3 as a function of the applied field. The amplitudes of the precessional modes φ_1, φ_2, φ_3 behave similarly. The amplitude of mode 1 rises exactly in the field range where an instability has been predicted from the analysis of the Floquet multipliers. At the first velocity bump, mode 1 has a large amplitude (3.5 nm) comparable to the DW width $\Delta = 3$ nm. Mode 2 has a maximum amplitude (0.7 nm) at the position of the second velocity bump but this amplitude is only 30% of mode 1. Modes 3 and mode 4 (not shown) have much smaller amplitudes. It is tempting to associate the velocity bumps at $h_n = 1.2$ and at $h_n = 2$ to the first and second modes, respectively. More information will be obtained from the dependence of the modes amplitudes on the damping parameter (see Sec. III D below).

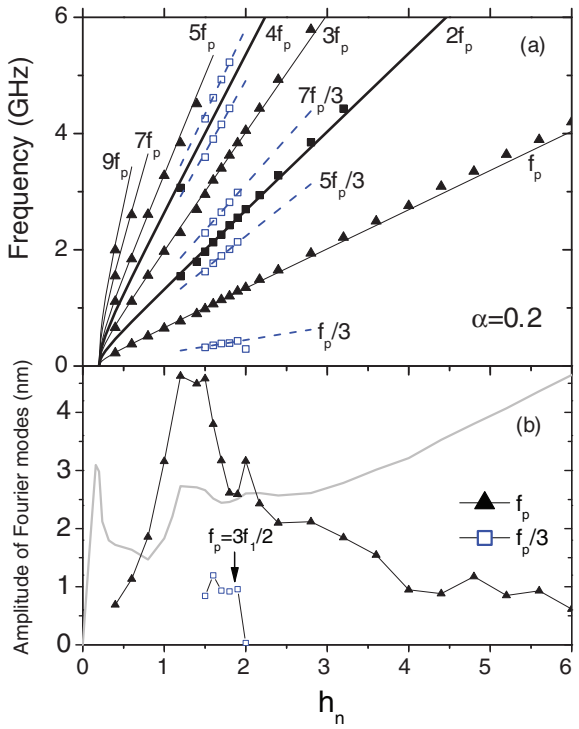

FIG. 8. (Color online) (a) Field dependence of the main frequencies in the Fourier spectrum of the amplitude of the first flexural mode $q_1(t)$ for $\alpha = 0.2$ and $d/\Lambda = 4$. The precession frequency $f_p = f_0/2$ and its overtones are represented by black symbols (the full and dotted lines represent the frequencies calculated within the 1D model). The subharmonic frequency $f_p/3$ and its overtones are represented by blue empty squares. (b) Amplitude of the two main frequencies f_p and $f_p/3$ (in gray, the velocity curve) in the Fourier spectrum of $q_1(t)$.

C. Fractional frequencies

Similarly to the results from the analytical model, the analysis of the Fourier spectrum of the $q_n(t)$ and $\varphi_n(t)$ components reveals the appearance of unexpected frequencies, namely subharmonics of the main frequency, in the field range of the velocity bumps $h_n = 1$–2. Figure 8(a) shows the field dependence of the main frequencies of the Fourier spectrum of $q_1(t)$. The fundamental frequency of $q_1(t)$ (and $\varphi_1(t)$) is the precessional frequency f_p which approaches $\gamma H/2\pi(1+\alpha^2)$ at high field ($H \gg H_W$). Many overtones of f_p are observed at low field as expected from Eq. (10). For the q_1 mode it is seen that the new frequencies can be expressed as $2nf_p \pm f_p/3$ with $n = 0, 1, 2$.

The amplitudes of the frequency components are obtained from the discrete Fourier transform of $q_n(t)$. As shown in Fig. 8(b) the amplitude of the $f_p/3$ component of q_1 reaches as much as 30% of the f_p component. The other components of the DW profile and precession q_0, φ_1, q_2, φ_2 also show fractional frequencies: $2nf_p/3$ (n an integer) for q_0, q_2, φ_2, and $nf_p/3$ for φ_1.

To summarize the results for $\alpha = 0.2$, one obtains velocity bumps above the Walker field. These bumps come with a large amplitude of the flexural and precessional modes (particularly the first ones) and fractional frequencies indicating a highly nonlinear behavior. The velocity bumps are consistent with experimental results in ferromagnetic semiconductors where either a bump or a velocity plateau is observed in this field range.[10,15] The velocity plateau could probably be better understood by taking into account additional DW flexural modes propagating along the plane of the DW and described by a $k_\parallel$ wave vector. The dispersion curves calculated for the static regime in Ref. 25 seem to suggest that the resonance frequency slightly increases with $k_\parallel$ starting from the $k_\parallel = 0$ value (calculated here). This would likely give a slightly more spread-out feature extending to higher fields.

Bumps at still higher fields (100 mT in GaMnAs, 50 mT in GaMnAsP) are also observed experimentally. As we shall see in the next section the study of the influence of the damping parameter will provide keys to understand these experimental findings.

D. Influence of the damping parameter

In order to investigate the effect of the damping, the micromagnetic simulations are performed for a smaller damping parameter $\alpha = 0.1$. Figure 9(a) shows the field dependence of the velocity for $\alpha = 0.1$. In addition to the two velocity bumps in the range $h_n = 1$–2, a new bump appears abruptly in the range $h_n = 5$–6. In this range the m_i components of the magnetization show a transient regime for several tens of nanoseconds before their oscillation amplitude stabilizes and the average velocity becomes time independent. The duration of the transient regime diverges at the onset of this high velocity regime $h_n = 5$. This is in very good agreement with the weak instability found for the second mode from the

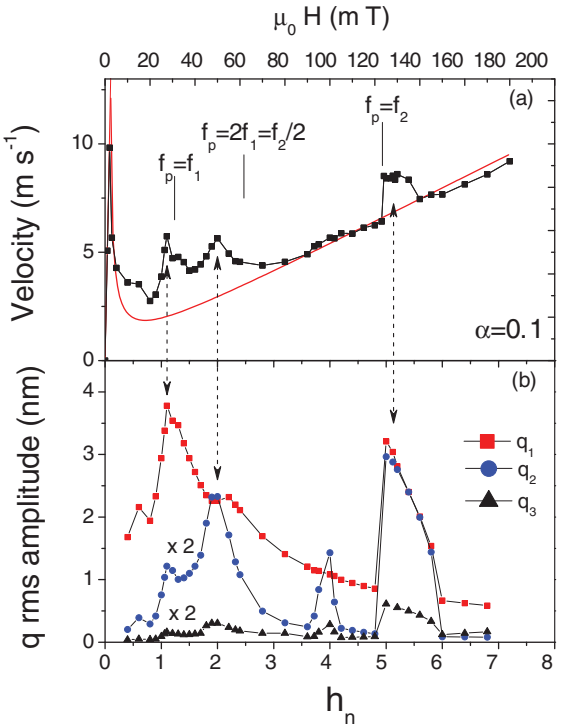

FIG. 9. (Color online) (a) DW velocity as a function of the applied magnetic field for a damping coefficient $\alpha = 0.1$ and $d/\Lambda = 4$, micromagnetic simulation (squares), 1D model (red line). (b) Amplitudes (rms values) of the first three flexural modes of the DW q_1, q_2, and q_3.

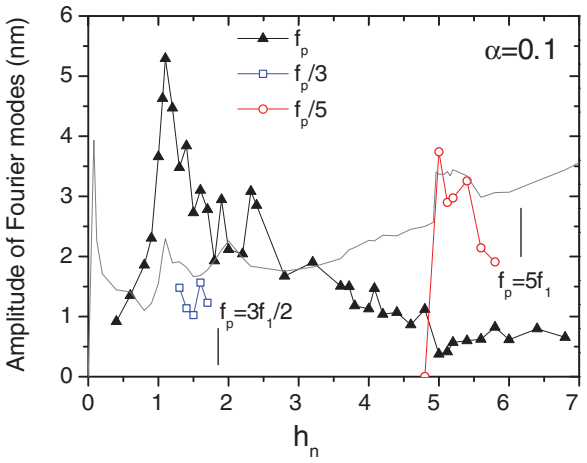

FIG. 10. (Color online) Amplitude of the main frequencies in the Fourier spectrum of the first flexural mode $q_1(t)$ for a damping coefficient $\alpha = 0.1$ and $d/\lambda = 4$ (in gray, the velocity curve).

Floquet multiplier precisely at $h_n = 5$ (Fig. 4). In order to know which flexural and precessional modes are involved in this high velocity regime we plot the amplitudes of the three first flexural modes in Fig. 9(b). Both the first and second modes have large amplitudes, q_1 being nevertheless larger than q_2 by a factor of about 2. Interestingly one can notice that the amplitude of the second mode also has a peak around $h_n = 4$, whereas the first mode amplitude decreases monotonously. However, in this range only a very small velocity enhancement is observed [Fig. 9(a)]. Therefore, in agreement with the considerations derived from the analytical model, we conclude that velocity enhancement is mainly related to the amplitude of the first mode.

In the field range of the velocity bumps fractional frequencies also clearly appear in the Fourier spectrum of the flexural and precessional modes. In the range $h_n = 1$–2, the results are similar to the case $\alpha = 0.2$: One observes the frequency $f_p/3$ and its overtones. As seen in Fig. 10 the amplitude of this frequency component in the q_1 mode reached about 30% of the f_p component. In the range $h_n = 5$–6 new fractional frequencies $pf_p/5$ with p up to 11 are observed. For the q_1 mode, the largest amplitude is now at $f_p/5$ (Fig. 10). The fractional frequencies $f_p/3$ and $f_p/5$ appear close to the field values where $f_p = 3f_1/2$ and $f_p = 5f_1$, respectively, which, as in the previous case with $\alpha = 0.2$, may explain the presence of such frequencies in the Fourier spectrum of the flexural modes.

To summarize we see that decreasing the damping parameter leads to an additional region of enhanced velocity, in agreement with experimental results, e.g., on ferromagnetic GaMnAs and GaMnAsP.[15] In our previous work only one velocity bump was found in the simulations. It was related to a large amplitude of the first flexural and precessional modes. We attributed this behavior to a resonant excitation of the first free-oscillation mode of the DW at the field corresponding to enhanced velocity. However the extension of simulations to smaller damping parameter in the present work shows a more complex situation with a large amplitude of the q_1 and φ_1 modes occurring in not one but several field ranges, as well as a large amplitude for the q_2 and φ_2 modes. Moreover we observe the appearance of fractional frequencies in the Fourier spectrum of the flexural and precessional modes.

IV. CONCLUSION

DW propagation has been studied in ferromagnetic layers with thickness larger than the exchange length where complex DW dynamics arises from the excitation of flexural modes. We have developed an analytical model for DW propagation taking into account DW flexing. The results of this model have been compared to DW dynamics obtained from the detailed analysis of time-resolved magnetic images from micromagnetic simulations. From the model we see that the most important parameters are the ratio of the layer thickness over the exchange length and the damping constant. We have determined the eigenfrequencies of the flexural modes. We have shown that the precessional regime of the DW motion is unstable with respect to flexing. This instability was found even when neglecting the action on the DW magnetization of the stray field from adjacent domains. The range of the field strength of the flexing instabilities is found by calculating the Floquet multipliers. The most important is the first flexing mode compatible with the natural boundary conditions. The instability range corresponds well to the field range where the precession frequency is close to the mode eigenfrequency and where large mode amplitudes are obtained by simulations. In some limited range of field strength the instability with respect to the second mode is possible. However the velocity bumps that arise from the effect of the stray field on the magnetization precession occur only for a large amplitude of the first mode for symmetry reasons. Decreasing the damping parameter yields additional regions of enhanced velocity.

At large mode amplitudes, due to the nonlinearity of the system, fractional frequencies appear as in parametric oscillators. It should be noted that here the forcing of the oscillators is not provided by an external periodic source but by the magnetization precession under constant applied field.

The analytical model and the micromagnetic simulations developed in this paper explain the main features of experimental velocity curves. The remaining discrepancies between some experimental curves and the calculated or simulated ones would probably be solved by taking into account flexural modes propagating in the DW plane. This would require a further extension of this $(q,\varphi,dq/dz,d\varphi/dz)$ dynamical model into a three-dimensional $(q,\varphi,\vec{\nabla} q,\vec{\nabla} \varphi)$ model. Besides, the extension of this model to the case of in-plane magnetization for which a number of experimental results exists for ferromagnetic semiconductor layers as well as metallic layers or stripes would also give insight into deviations from the simple 1D model.

ACKNOWLEDGMENTS

This work was performed in the framework of the ANR-MANGAS project (ANR 2010-BLANC-0424-02). One of us (A.C.) acknowledges financial support from CNRS (France) as invited researcher.

[1]D. A. Allwood, G. Xiong, C. C. Faulkner, D. Atkinson, D. Petit, and R. P. Cowburn, Science **309**, 1688 (2005).
[2]S. S. P. Parkin, M. Hayashi, and L. Thomas, Science **320**, 190 (2008).
[3]J. C. Slonczewski, J. Appl. Phys. **44**, 1759 (1973).
[4]N. L. Schryer and L. R. Walker, J. Appl. Phys. **45**, 5406 (1974).
[5]A. P. Malozemoff and J. C. Slonczewski, *Magnetic domain walls in bubble materials* (Academic Press, New York, 1979).
[6]S. Lemerle, J. Ferré, C. Chappert, V. Mathet, T. Giamarchi, and P. Le Doussal, Phys. Rev. Lett. **80**, 849 (1998).
[7]P. J. Metaxas, J. P. Jamet, A. Mougin, M. Cormier, J. Ferré, V. Baltz, B. Rodmacq, B. Dieny, and R. L. Stamps, Phys. Rev. Lett. **99**, 217208 (2007).
[8]M. Yamanouchi, J. Ieda, F. Matsukura, S. E. Barnes, S. Maekawa, and H. Ohno, Science **317**, 1726 (2007).
[9]S. E. Barnes, J. Eckmann, T. Giamarchi, and V. Lecomte, Nonlinearity **25**, 1427 (2012).
[10]A. Dourlat, V. Jeudy, A. Lemaître, and C. Gourdon, Phys. Rev. B **78**, 161303 (2008).
[11]C. Gourdon, V. Jeudy, A. Cebers, A. Dourlat, K. Khazen, and A. Lemaître, Phys. Rev. B **80**, 161202 (2009).
[12]G. S. D. Beach, C. Knutson, C. Nistor, M. Tsoi, and J. L. Erskine, Phys. Rev. Lett. **97**, 057203 (2006).
[13]R. Moriya, M. Hayashi, L. Thomas, C. Rettner, and S. S. P. Parkin, Appl. Phys. Lett. **97**, 142506 (2010).
[14]C. Zinoni, A. Vanhaverbeke, P. Eib, G. Salis, and R. Allenspach, Phys. Rev. Lett. **107**, 207204 (2011).
[15]L. Thevenard, C. Gourdon, S. Haghgoo, J.-P. Adam, H. J. von Bardeleben, A. Lemaître, W. Schoch, and A. Thiaville, Phys. Rev. B **83**, 245211 (2011).
[16]K. Yamada, J.-P. Jamet, Y. Nakatani, A. Mougin, A. Thiaville, T. Ono, and J. Ferré, Appl. Phys. Exp. **4**, 113001 (2011).
[17]O. A. Tretiakov, D. Clarke, Gia-Wei Chern, Ya. B. Bazaliy, and O. Tchernyshyov, Phys. Rev. Lett. **100**, 127204 (2008).
[18]D. J. Clarke, O. A. Tretiakov, G.-W. Chern, Ya B. Bazaliy, and O. Tchernyshyov, Phys. Rev. B **78**, 134412 (2008).
[19]A. Pikovsky, M. Rosenblum, and J. Kurths, *Synchronization* (Cambridge University Press, Cambridge, England, 2001).
[20]T. T. Fang and A. A. Thiele, J. Appl. Phys. **69**, 4593 (1991).
[21]E. Magyary and H. Thomas, Z. Phys. B **59**, 167 (1985).
[22]R. M. Hornreich and H. Thomas, Phys. Rev. B **17**, 1406 (1978).
[23]D. Bouzidi and H. Suhl, Phys. Rev. Lett. **65**, 2587 (1990).
[24]S. W. Yuan and H. N. Bertram, J. Appl. Phys. **69**, 5874 (1991).
[25]J. C. Slonczewski, J. Magn. Magn. Mater. **23**, 305 (1981).
[26]S. H. Strogatz, *Nonlinear dynamics and chaos* (Persius Books, Cambridge, MA, USA, 1994).
[27]D. Garcia-Alvarez, A. Stefanovska, and P. V. E. McClintock, Phys. Rev. E **77**, 056203 (2008).
[28]F. B. Hagedorn, J. Appl. Phys. **45**, 3129 (1974).
[29]Ar. Abanov and V. L. Pokrovsky, Phys. Rev. B **58**, R8889 (1998).
[30]P. Bergé, Y. Pommeau, and C. Vidal, *Order within Chaos* (Wiley, New York, 1984).
[31]S. Petit-Watelot, J.-V. Kim, A. Ruotolo, R. M. Otxoal, K. Bouzehouane, J. Grollier, A. Vansteenkiste, B. Van de Wiele, V. Cros, and T. Devolder, Nat. Phys. **8**, 682 (2012).
[32]OOMMF is available at http://math.nist.gov/oommf.
[33]C. Gourdon, A. Dourlat, V. Jeudy, K. Khazen, H. J. von Bardeleben, L. Thevenard, and A. Lemaître, Phys. Rev. B **76**, 241301(R) (2007).